Received: 16 November 2021 | Revised: 2 December 2021 | Accepted: 3 December 2021

DOI: 10.1002/ardp.202100450

FULL PAPER

ARCH PHARM DPhG
Archiv der Pharmazie

Design, synthesis, biological activity, molecular docking, and molecular dynamics of novel benzimidazole derivatives as potential AChE/MAO-B dual inhibitors

Derya Osmaniye[1,2] | Asaf E. Evren[1,3] | Begüm N. Sağlık[1,2] | Serkan Levent[1,2] | Yusuf Özkay[1,2] | Zafer A. Kaplancıklı[1]

[1]Department of Pharmaceutical Chemistry, Faculty of Pharmacy, Anadolu University, Eskişehir, Turkey

[2]Doping and Narcotic Compounds Analysis Laboratory, Faculty of Pharmacy, Anadolu University, Eskişehir, Turkey

[3]Vocational School of Health Services, Department of Pharmacy Services, Bilecik Şeyh Edebali University, Bilecik, Turkey

Correspondence
Derya Osmaniye, Department of Pharmaceutical Chemistry, Faculty of Pharmacy, Anadolu University, 26470 Eskişehir, Turkey.
Email: dosmaniye@anadolu.edu.tr

Abstract

To develop new acetylcholinesterase (AChE)–monoamine oxidase-B (MAO-B) dual inhibitors against Alzheimer's disease, the benzimidazole ring, which has a propargyl side chain with previously proven selective MAO-B inhibitory activity, was used as the main structure. Moreover, like donepezil, it was thought that the enzyme AChE would provide π–π interactions with the peripheral anionic side in this structure. Piperazine derivatives were chosen for the cationic active site. The synthesis of the compounds was carried out in five steps. The structures of the compounds were determined using ^{1}H-NMR (nuclear magnetic resonance), ^{13}C-NMR, and high-resolution mass spectrometry spectroscopic methods. First, the in vitro AChE, butyrylcholinesterase (BChE), MAO-A, and MAO-B inhibitory potentials of the obtained compounds were investigated. As a result of activity tests, compounds **5b**, **5e**, **5g**, and **5h** showed inhibitory activity against AChE; compounds **5e** and **5g** showed inhibitory activity against MAO-B. None of the compounds showed inhibitory activity against BChE or MAO-A. Compounds **5e** and **5g** showed dual inhibition. Among these compounds, compound **5g** had inhibition potential similar to that of donepezil and selegiline. For compound **5g**, further kinetic studies and Aβ-plaque inhibitory potentials were investigated using in vitro methods. Molecular docking studies were performed using both AChE and *h*MAO-B crystals to elucidate the compound's interactions with the enzyme active site. The binding modes of the compound on AChE were fully elucidated by molecular dynamics studies.

KEYWORDS
Alzheimer's disease, benzimidazole, molecular docking, molecular dynamics, propargyl

1 | INTRODUCTION

Alzheimer's disease (AD) is a progressive neurodegenerative brain disorder that affects the elderly population. This disorder is the most common form of dementia and is generally diagnosed in individuals over the age of 65 years; it is characterized by memory deterioration, behavioral changes, and impaired cognitive functions.[1,2] Although tremendous advances have been made in the study of the pathogenesis of AD since its discovery, unfortunately, scientists have yet to fully elucidate its pathology.[3] AD has been recognized as a highly

complex and multifactorial disease. Various molecular mechanisms, including neurotransmitter system dysfunction, deposition of intracellular neurofibrillary tangles, metal ion dyshomeostasis, extracellular senile plaques possessing amyloid-β (Aβ) proteins, oxidative stress, τ-protein hyperphosphorylation, mitochondria dysfunction, and neuronal dysfunction, are closely related to the occurrence and development of AD.[4,5]

To date, clinical Food and Drug Administration (FDA)-approved anti-AD drugs mainly concentrate on acetylcholinesterase (AChE) inhibitors, for instance, rivastigmine, donepezil, and galantamine. These drugs restore cognitive functions and alleviate the symptoms of AD by enhancing the level of acetylcholine (ACh).[6] Neurodegenerative processes that predominantly affect the cholinergic system result in low ACh levels, which inhibit learning processes and memory formation. The most important method developed to increase ACh concentration and improve cholinergic transmission is the inhibition of cholinesterases (ChEs), which catalyze the breakdown of ACh.[2,7] The enzymatic cavity of AChE is characterized by a nearly 20-Å deep narrow gorge composed of two binding sites: the catalytic active site (CAS) at the bottom and the peripheral anionic site (PAS) near the entrance of the gorge.[8]

Another important contributor to the progress in AD is the catabolism of monoamine.[9] The activities of monoamine oxidases (MAO) were significantly increased in AD patients, leading to an increase in ROS production, neuroinflammation, and Aβ deposition.[10] The neurotoxic products catalyzed by MAO-B, such as hydrogen peroxide, promote the formation of ROS and cause neuronal damage. Therefore, the development of an MAO-B inhibitor is a potential option for the treatment of AD.[11–13]

Most drugs approved by the FDA for use in AD have a heterocyclic system; this is evidence of the activity of heterocyclic-based compounds to inhibit ChEs. In addition, studies have proven that compounds with tricyclic and heterocyclic systems can interact with each CAS and PAS of ChEs through hydrophobic interactions.[14] To interact with the PAS region, a heterocyclic system that can be used instead of indanone in donepezil agent was needed. The benzimidazole scaffold represents a privileged structure because of its presence in inhibitory potential against AD.[15–23] When the literature is reviewed, it is seen that compounds containing the propargylamine group show inhibitory potential against MAO enzyme and these compounds are used as multifunctional agents against Alzheimer's disease.[24–27]

Additionally, in our previous study, new *N*′-(arylidene)-4-[1-(prop-2-yn-1-yl)-1*H*-benzo[*d*]imidazol-2-yl]benzohydrazide derivatives were synthesized for their in vitro MAO-B inhibition potentials. Some of the compounds showed strong MAO-B inhibition.[28] In this study, several modifications to these compounds were made in accordance with the active site of AChE, and novel dual inhibitors were planned. The benzimidazole structure to which the propargyl group is attached was kept constant and it was thought that this region would also be in the PAS part of the active site of AChE. For the CAS region of the enzyme, piperazine derivatives were used instead of piperidine in the donepezil molecule. Here, it is planned to examine the activity contribution of both piperazine and substituents by using different substituents and derivatives without piperazine. The cholinergic residue was added to one molecule to strengthen the interaction with the CAS region and, therefore, the AChE inhibition potential was expected to increase.

2 | RESULTS AND DISCUSSION

2.1 | Chemistry

The compounds **5a–k** were obtained as presented in Scheme 1. Initially, a benzimidazole derivative (**1**) was obtained by means of the reaction between benzene-1,2-diamine and methyl 4-formylbenzoate using a ring closure reaction. Further, 3-bromoprop-1-yne was added to the structure using NaH. Ester hydrolysis was carried out using a 3:1 mixture of water/HCl (37%). Thionyl chloride was used to convert the carboxylic acid group to acyl halide. The work with the material was done under a fume hood. Finally, the resulting products were obtained by reacting the acyl halide with secondary amine derivatives. The structures of the compounds obtained were established by spectroscopic methods, namely, ^{1}H-NMR (nuclear magnetic resonance), ^{13}C-NMR, and high-resolution mass spectrometry (HRMS) (Supporting Information Data).

We generally encounter the following results: the terminal proton of the propynyl group was recorded at around 3.52 ppm and the other two protons of the same group were seen at around 5.20 ppm as a singlet. While piperazine protons were observed as three different peaks as broad singlets, imidazole protons showed two different multiple peaks. Benzene hydrogens were observed as two doublets with the coupling constant 8.3–8.4 Hz. Significant carbon values in ^{13}C-NMR can be shown for carbonyl and propynyl. Carbonyl carbon was recorded at 168 ppm and propynyl carbons were at 35, 77, and 78 ppm. The other carbons were observed between 6 ppm and 63 ppm for aliphatic carbons and between 111 ppm and 153 ppm for aromatic carbons. High-resolution mass spectroscopy analysis was also performed and all results were found in 5 ppm differences maximum.

2.2 | Biological activity

2.2.1 | Cholinesterase enzymes inhibition assay

The inhibitory activities of all obtained chalcone derivatives (**3**, **4**, **5a–k**) against cholinesterase enzymes were evaluated using the previously described in vitro modified Ellman's spectrophotometric method.[29–37]

The assay was completed in two steps. The first step was achieved by means of all the original compounds (**3**, **4**, **5a–k**) and reference agents, namely, donepezil and tacrine, at concentrations of 1000 and 100 μM. The enzyme activity results of the first step are presented in Table 1. Next, the selected compounds that displayed more than 50% inhibitory activity at concentrations of 1000 and

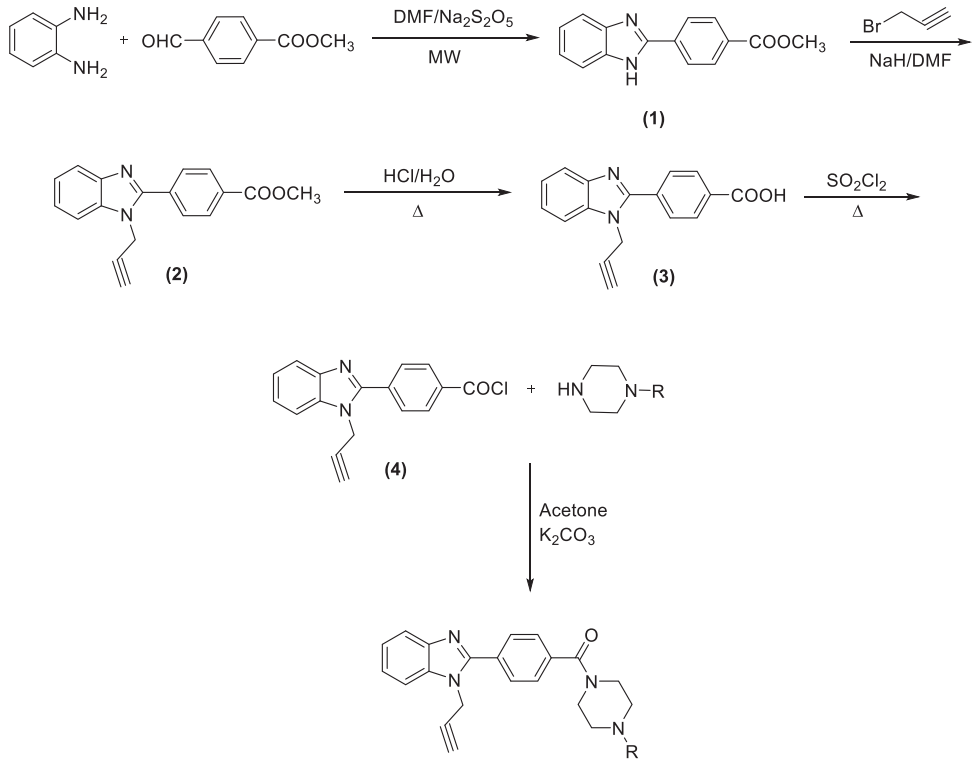

Compounds	R
5a	-Methyl
5b	-Ethyl
5c	2-Methoxyethyl
5d	-Isopropyl
5e	-Allyl
5f	-Formyl
5g	-2-(Dimethylamino)ethyl
5h	-3-(Dimethylamino)propyl
5i	-Cyclopropyl
5j	-Cyclohexyl
5k	-4-Nitrophenyl

SCHEME 1 The synthetic route to the target compounds **5a–k**

100 μM were further tested, along with the reference agents, at concentrations of 10–0.001 μM. The IC_{50} values of the test compounds and reference agents are presented in Table 2.

As a result of the enzyme inhibition test, it was observed that all compounds were more effective against AChE. None of the compounds exhibited greater than 50% inhibitory activity against butyrylcholinesterase (BChE) in the first step. Compounds **5b**, **5e**, **5g**, and **5h** displayed greater than 50% inhibitory activity at 10^{-4} M concentrations. These compounds contain ethyl, allyl, 2-dimethylaminoethyl, and 3-dimethylaminopropyl substituents, respectively. As a result of the tests performed in the second step, the derivative carrying 2-dimethylaminoethyl (**5g**) was the most active derivative, with a value of IC_{50} = 0.022 μM. This value is very similar to the IC_{50} value of donepezil (IC_{50} = 0.021).

When the structure-activity relationship is examined, the following observations can be made:

- Derivatives without a piperazine ring (**3** and **4**) showed lower activity than those containing a piperazine ring.
- Derivatives with a bulky aromatic or cyclic aliphatic structure on the piperazine ring also showed less activity than those with a straight chain.
- Ethyl residue among the straight-chain alkyl substituents positively affected the activity.
- The activity increased with the addition of dimethylamine to this ethyl residue.
- The activity decreased when dimethylaminopropyl was used instead of dimethylaminoethyl.

TABLE 1 % Inhibition of the synthesized compounds, donepezil, tacrine, moclobemide, and selegiline against ChE and MAO enzymes

Compounds	AChE % inhibition		BChE % inhibition		MAO-A % inhibition		MAO-B % inhibition	
	10^{-3} M	10^{-4} M	10^{-3} M	10^{-4} M	10^{-3} M	10^{-4} M	10^{-3} M	10^{-4} M
3	**65.389 ± 1.548**	40.375 ± 0.897	39.652 ± 0.985	31.218 ± 0.854	35.216 ± 0.720	27.120 ± 0.865	**51.565 ± 1.024**	40.951 ± 0.893
4	**67.021 ± 1.230**	44.112 ± 0.901	42.457 ± 0.893	35.095 ± 0.902	38.494 ± 0.912	28.749 ± 0.745	**58.592 ± 0.975**	42.735 ± 0.912
5a	**72.654 ± 1.054**	42.735 ± 0.884	35.669 ± 0.715	28.046 ± 0.842	30.645 ± 0.890	20.843 ± 0.621	**69.749 ± 1.147**	46.448 ± 0.721
5b	**96.205 ± 1.623**	**85.486 ± 1.104**	42.039 ± 0.934	36.798 ± 0.856	34.749 ± 0.893	27.558 ± 0.714	**70.594 ± 1.165**	48.912 ± 0.997
5c	**76.950 ± 1.175**	42.975 ± 0.923	38.495 ± 0.855	30.114 ± 0.810	33.942 ± 0.822	24.055 ± 0.860	**64.741 ± 0.945**	40.913 ± 0.892
5d	**82.654 ± 1.005**	46.021 ± 0.875	41.065 ± 0.714	33.795 ± 0.932	36.456 ± 0.817	27.403 ± 0.792	**58.647 ± 0.846**	37.842 ± 0.726
5e	**90.352 ± 1.106**	**82.123 ± 1.117**	44.748 ± 0.930	39.044 ± 0.756	32.735 ± 0.812	21.195 ± 0.875	**94.027 ± 1.588**	**88.912 ± 1.372**
5f	**78.912 ± 1.627**	40.197 ± 0.769	36.003 ± 0.813	30.841 ± 0.818	32.146 ± 0.763	23.942 ± 0.819	**67.492 ± 1.002**	39.588 ± 0.821
5g	**96.246 ± 1.248**	**90.475 ± 1.490**	43.774 ± 0.901	35.612 ± 0.701	34.475 ± 0.749	30.612 ± 0.820	**98.566 ± 1.402**	**93.476 ± 1.378**
5h	**91.588 ± 1.114**	**80.364 ± 1.375**	38.645 ± 0.892	31.662 ± 0.825	30.185 ± 0.770	24.733 ± 0.732	**75.826 ± 1.116**	47.492 ± 0.809
5i	**80.617 ± 1.050**	47.495 ± 0.826	46.495 ± 0.932	37.456 ± 0.862	35.497 ± 0.890	30.499 ± 0.791	**69.667 ± 1.004**	41.645 ± 0.874
5j	**76.441 ± 1.107**	46.127 ± 0.912	42.084 ± 0.874	30.226 ± 0.755	32.620 ± 0.806	26.902 ± 0.791	**62.473 ± 0.875**	43.942 ± 0.932
5k	**72.475 ± 1.452**	40.911 ± 0.881	45.112 ± 0.921	35.014 ± 0.827	36.795 ± 0.768	28.175 ± 0.613	**69.881 ± 0.892**	44.919 ± 0.902
Donepezil	99.254 ± 2.104	97.426 ± 1.890	-	-	-	-	-	-
Tacrine	-	-	98.255 ± 1.895	95.465 ± 1.344	-	-	-	-
Moclobemide	-	-	-	-	94.121 ± 2.760	82.143 ± 2.691	-	-
Selegiline	-	-	-	-	-	-	99.387 ± 1.385	95.629 ± 1.456

Abbreviations: AChE, acetylcholinesterase; BChE, butyrylcholinesterase; MAO, monoamine oxidase.

TABLE 2 IC_{50} values of **5b**, **5e**, **5g**, **5h**, donepezil, and selegiline against AChE and MAO-B enzymes

Compounds	10^{-3} M	10^{-4} M	10^{-5} M	10^{-6} M	10^{-7} M	10^{-8} M	10^{-9} M	IC_{50} (μM)
AChE % inhibition								
5b	96.205 ± 1.623	85.486 ± 1.104	76.649 ± 1.112	70.148 ± 1.240	63.199 ± 1.247	46.520 ± 0.820	25.490 ± 0.721	0.046 ± 0.002
5e	90.352 ± 1.106	82.123 ± 1.117	76.912 ± 0.975	71.651 ± 1.126	57.499 ± 0.890	38.074 ± 0.802	29.507 ± 0.723	0.103 ± 0.004
5g	**96.246 ± 1.248**	**90.475 ± 1.490**	**82.492 ± 1.385**	**73.033 ± 1.118**	**64.818 ± 1.389**	**48.983 ± 0.897**	**21.267 ± 0.729**	**0.024 ± 0.001**
5h	91.588 ± 1.114	80.364 ± 1.375	76.493 ± 1.402	70.811 ± 1.248	60.035 ± 1.056	45.729 ± 0.999	30.654 ± 0.726	0.084 ± 0.003
Donepezil	99.254 ± 2.104	97.426 ± 1.890	92.258 ± 1.510	90.318 ± 1.104	81.365 ± 1.104	43.875 ± 0.601	21.418 ± 0.548	0.021 ± 0.001
MAO-B % inhibition								
5e	94.027 ± 1.588	88.912 ± 1.372	80.627 ± 1.402	73.248 ± 1.108	58.033 ± 0.995	35.942 ± 0.842	22.249 ± 0.723	0.093 ± 0.003
5g	**98.566 ± 1.402**	**93.476 ± 1.378**	**88.024 ± 1.140**	**85.034 ± 1.477**	**76.191 ± 1.057**	**43.651 ± 0.907**	**34.449 ± 0.768**	**0.041 ± 0.002**
Selegiline	99.387 ± 1.385	95.629 ± 1.456	86.205 ± 1.200	78.324 ± 1.108	66.871 ± 1.056	42.875 ± 0.865	16.748 ± 0.596	0.037 ± 0.001

Abbreviations: AChE, acetylcholinesterase; MAO, monoamine oxidase.

2.2.2 | MAO enzymes inhibition assay

The inhibition power on MAO isoenzymes of the synthesized compounds was evaluated by using the in vitro fluorometric method described previously by our research group.[38–44] The results of the first step of the enzyme activity assay are given in Table 1 and those of the second step in Table 2. The second step was performed with further concentrations (by serial dilutions ranging from 10^{-5} to 10^{-9} M) of the reference drug and selected derivatives that showed more than 50% inhibitory activity at 10^{-4} M concentration. Therefore, the half-maximal inhibitory concentration (IC_{50}) values of the selected compounds **5e** and **5g** and the reference inhibitor were calculated and these results are given in Table 2.

It was understood by analyzing Table 1 that some of the synthesized compounds in the series showed remarkable inhibition potency at 10^{-3} M concentration; however, none of them displayed significant inhibitory activity at 10^{-4} M concentration against MAO-A. It was seen that all obtained derivatives had higher inhibition rates on MAO-B than on MAO-A. Therefore, it was concluded that all synthesized compounds showed selective MAO-B inhibitory activity. All compounds displayed more than 50% inhibitory activity at 10^{-3} M concentration, while compounds **5e** and **5g** had more than 50% inhibitory activity at 10^{-4} M concentration for MAO-B, and thus, the second step of the enzyme inhibition assay was carried out using further dilutions of these compounds. Compound **5g** was found to be the most effective agent in the series, with an IC_{50} value of 0.041 ± 0.002 μM. Furthermore, it was noteworthy that this compound showed a degree of inhibition very similar to that of the reference drug selegiline (IC_{50} value = 0.037 ± 0.001 μM).

2.2.3 | Enzyme kinetics studies of ChE and MAO enzymes

Enzyme kinetics studies were performed using a procedure similar to the ChE and MAO enzyme inhibition assay and the mechanisms of AChE and MAO-B inhibition were determined. Compound **5g**, which was the most potent agent on both AChE and MAO-B enzymes, was included in these studies.

To estimate the type of inhibition of this compound, linear Lineweaver–Burk graphs were used. Substrate velocity curves in the absence and presence of compound **5g** were recorded. This compound was prepared at concentrations of $IC_{50}/2$, IC_{50}, and $2 \times IC_{50}$ for the enzyme kinetic studies. For AChE enzymes, the substrate (acetylthiocholine iodide) solution was used with serial dilutions at six different concentrations (600, 300, 150, 75, 37.5, and 18.75 μM). For MAO-B enzymes, the substrate (tyramine) solution was prepared at six different concentrations (range 20–0.625 μM). The secondary plots of the slope (K_m/V_{max}) versus varying concentrations (0, $IC_{50}/2$, IC_{50}, and $2 \times IC_{50}$) were created to calculate the K_i (intercept on the *x*-axis) value of this compound. The graphical analyses of the steady-state inhibition data for compound **5g** are shown in Figures 1 and 2.

Enzyme inhibition is typically divided into two categories as reversible and irreversible. In irreversible inhibition, the inhibitor binds to an enzyme either covalently or forms a recalcitrant complex structure. The reversible inhibition category is also divided into four types: mixed type, competitive, noncompetitive, and uncompetitive inhibition types. The type of inhibition at Lineweaver–Burk graphs is defined as uncompetitive if four lines are parallel, competitive if the lines intersect on axis *y*, noncompetitive if the lines intersect on axis *x*, and as mixed if four lines are within the areas of the graphic but out of any axis. According to the Lineweaver–Burk plots, a graph with lines that do not intersect at the *x*-axis or the *y*-axis is formed for mixed-type inhibition. Therefore, as shown in Figure 1, compound **5g** was reversible and had mixed-type inhibitors with inhibition features similar to those of the substrates. The K_i value for compound **5g** was 0.019 μM for inhibition of AChE. Also, it was seen from Figure 2 that four lines intersect on the *x*-axis. According to Lineweaver–Burk curves, compound **5g** against MAO-B enzyme showed noncompetitive inhibition. The K_i value for compound **5g** was calculated as 0.034 μM for inhibition of MAO-B.

It is known that irreversible enzymatic inhibition involves covalent interactions between substrate and enzyme. Inhibition involving noncovalent interactions, such as hydrophobic interactions, ionic bonds, and hydrogen bonds is reversible inhibition. In this type of inhibition, the inhibitors bind to the enzymes without forming any chemical bonds; thus, the enzyme–inhibitor complex can dissociate rapidly because noncovalent interactions can form rapidly and be broken easily. These noncovalent binding capabilities make reversible inhibitors with a lower risk of side effects than irreversible inhibitors. Consequently, compound **5g**, whose inhibition type was determined to be the reversible-mixed type for AChE and reversible-noncompetitive inhibition for MAO-B, is of pharmaceutical importance as a candidate inhibitor of AChE and MAO-B enzymes.

2.2.4 | Inhibition of β-amyloid 1–42 (Aβ42) aggregation

In addition to the decrease in cholinergic transmission in Alzheimer's patients, amyloid plaque accumulation consisting of β-amyloid (Aβ) peptides can be considered among the important causes. Recent studies have shown that two β-amyloid peptides (Aβ [1–40] and Aβ [1–42]) are present in the brain tissues, cerebrospinal fluid, and

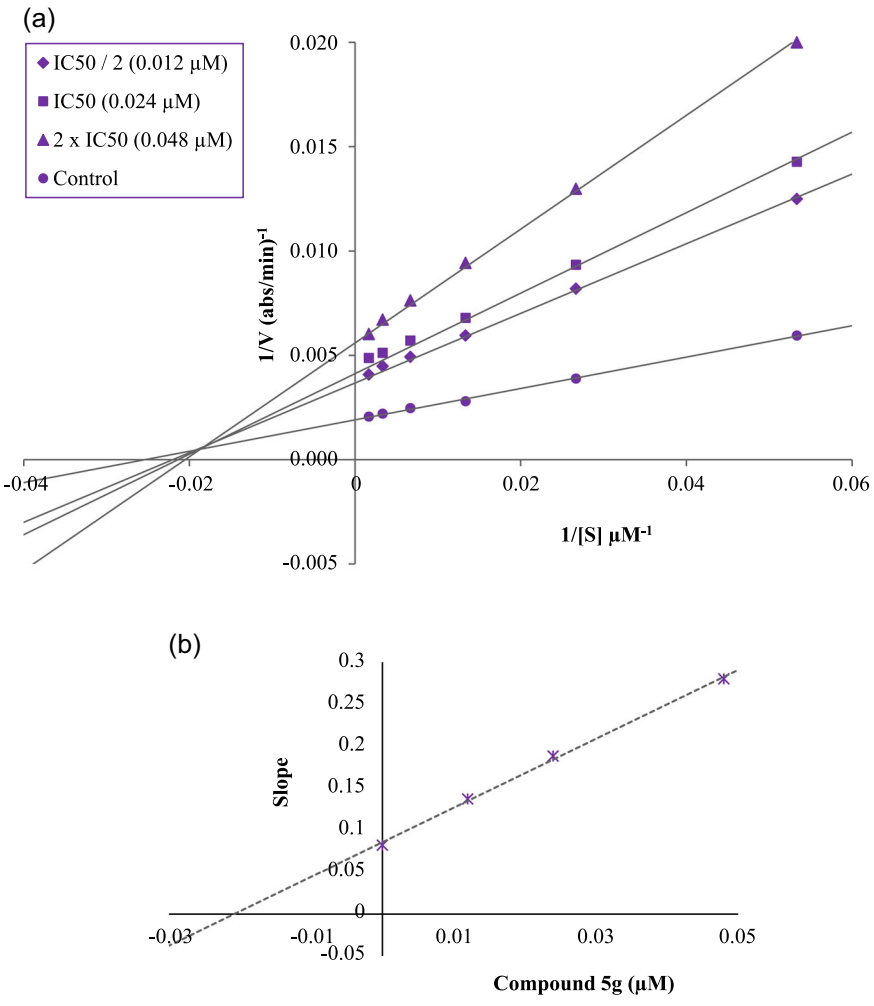

FIGURE 1 (a) Lineweaver–Burk plots for the inhibition of acetylcholinesterase by compound **5g**. [S], substrate concentration (μM); *V*, reaction velocity (1/*V* [abs/min]$^{-1}$). Inhibitor concentrations are shown at the left. (b) Secondary plot for the calculation of the steady-state inhibition constant (K_i) of compound **5g**. K_i was calculated as 0.019 μM

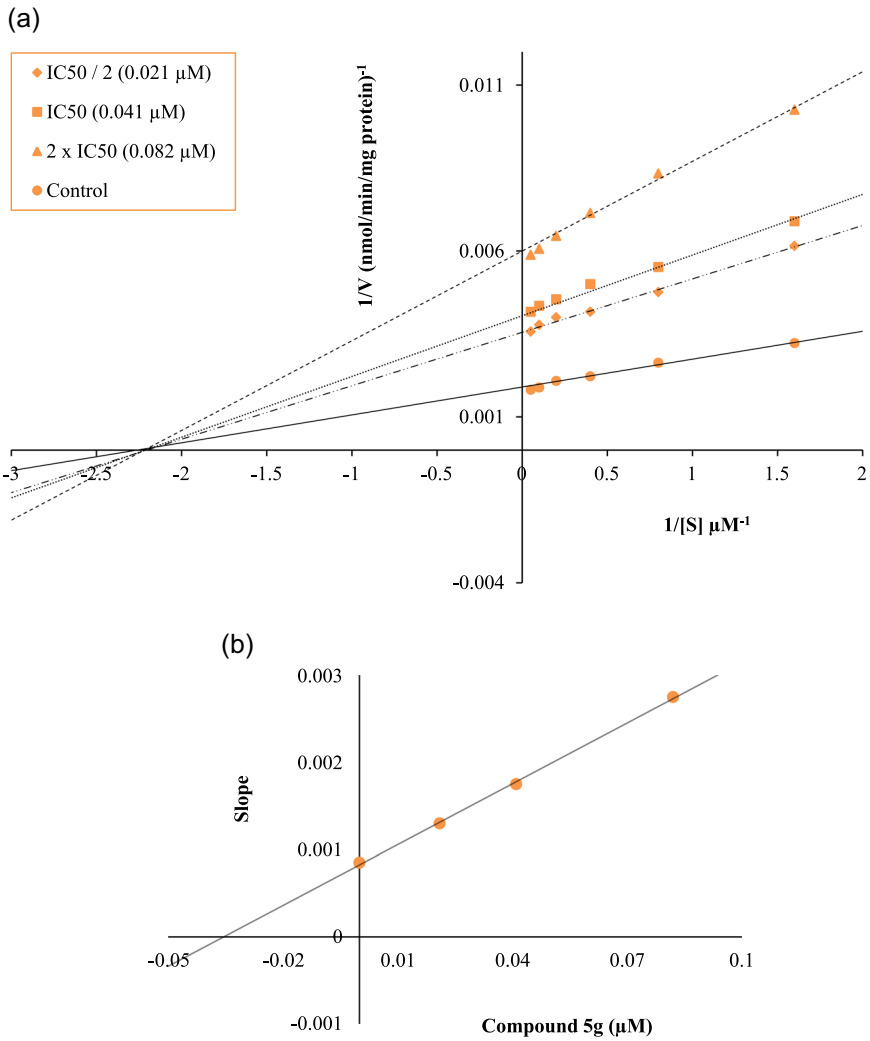

FIGURE 2 (a) Lineweaver–Burk plots for the inhibition of monoamine oxidase-B by compound **5g**. [S], substrate concentration (µM); *V*, reaction velocity (1/*V* [abs/min]$^{-1}$). Inhibitor concentrations are shown at the left. (b) Secondary plot for the calculation of the steady-state inhibition constant (K_i) of compound **5g**. K_i was calculated as 0.034 µM

plasma of patients suffering from AD. Hence, in the present study, for the selected compound **5g**, which displayed potent inhibitory activity against AChE, the inhibition of β-amyloid 1–42 (Aβ42) aggregation was evaluated using the β-amyloid 1–42 (Aβ42) ligand screening assay kit (BioVision). The test kit, based on the fluorometric method, was used in accordance with the recommended procedure. If an Aβ42 ligand is present, this reaction is inhibited/destroyed, thereby reducing or completely eliminating fluorescence. The percent inhibition of β-amyloid 1-42 (Aβ42) peptide aggregation is given in Figure 3 for compound **5g**, donepezil, and curcumin (reference drugs). These compounds were tested at concentrations of 10, 1, 0.1, and 0.01 µM. All test compound concentrations were applied in quadruplicate on the plates.

Corresponding to Figure 3, compound **5g** displayed more than 50% inhibition at a concentration of 10–0.1 µM. Compound **5g** showed inhibition at this concentration as follows: 86.11%, 81.29%, 62.77%, and 46.28%, respectively. Also, it was seen that compound **5g** displayed higher inhibition than curcumin; whereas it showed inhibition profile at a similar rate with donepezil.

2.3 | Molecular docking studies

After the determination of the active compound, we performed the docking study. The results showed that there were three π–π interactions between **5g** and AChE. Two of them were between the benzimidazole ring of the ligand and Trp286 and the last one was between the phenyl ring of the ligand and Tyr341. There was also a π–cation interaction between the quaternary amine of the ligand and Trp86. Moreover, one salt bridge and one H-bond were formed between the quaternary amine of **5g** and Glu202. All these interactions are shown in Figure 4. Additionally, there was an aromatic H-bond between H_7 of benzimidazole of compound **5g** and Ser293 (Figure 5).

The results showed that there were a lot of interactions between **5g** and the enzyme *h*MAO-B. The data obtained were examined and the two-dimensional (2D) and three-dimensional poses are displayed in Figure 6 and Figure 7. The results showed that there were two hydrophobic interactions (one was π–π, the other was π–cation) between **5g** and the enzyme. These interactions were determined between the benzimidazole ring of **5g** and Trp119 and the quaternary

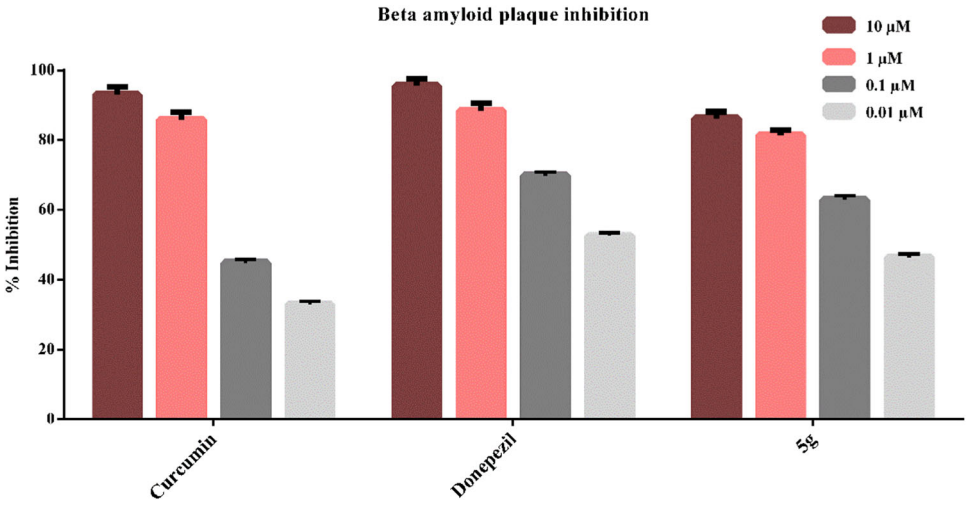

FIGURE 3 Beta amyloid plaque inhibition (%) of compound **5g**

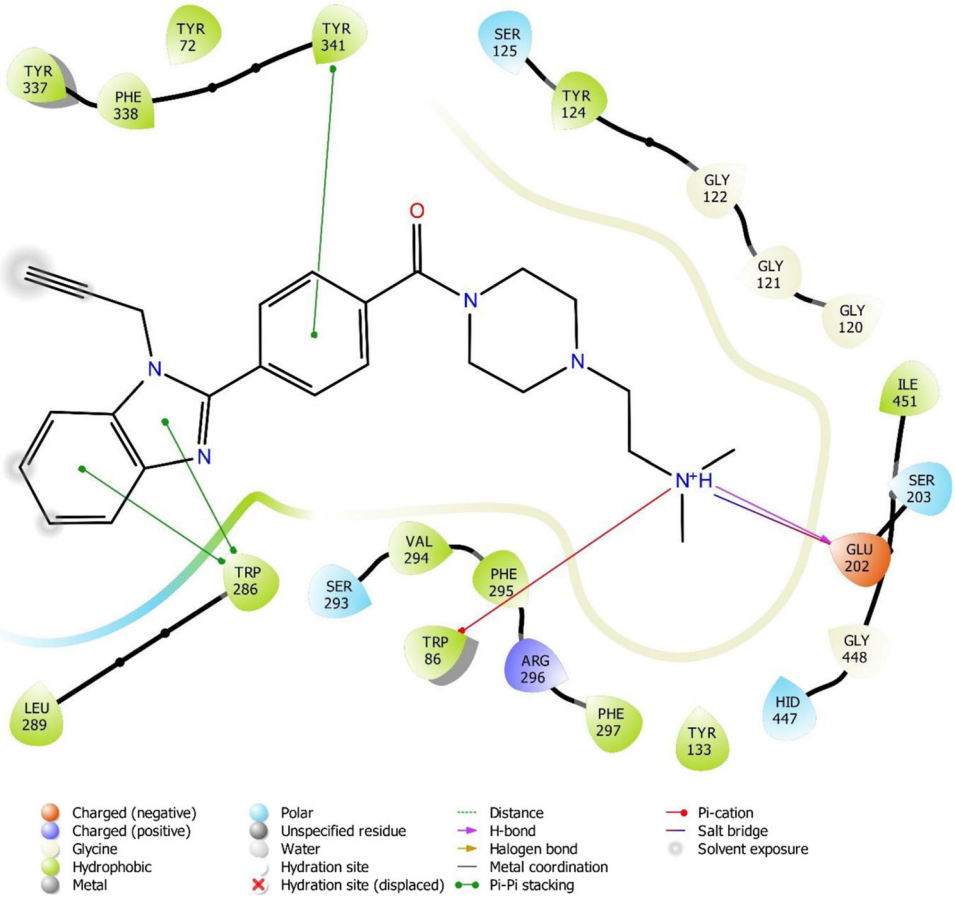

FIGURE 4 Two-dimensional interaction of compound **5g** at the binding region (PBDID: 4EY7)

ammonium of **5g** and Tyr398, respectively. Additionally, one H-bond and one aromatic H-bond were formed between the carbonyl oxygen of **5g** and Tyr345 and the phenyl of **5g** and Gln206. These interactions confirmed that **5g** fit well into the active region; therefore, the in vitro enzyme study and in silico study were found to be in harmony.

2.4 | Molecular dynamic simulation (MDS) studies

First, the MDS data were checked for the stability of the ligand–enzyme complex during the simulation (Figure 8). The plot of the radius of gyration (Rg) versus time (ns), the plot of root mean

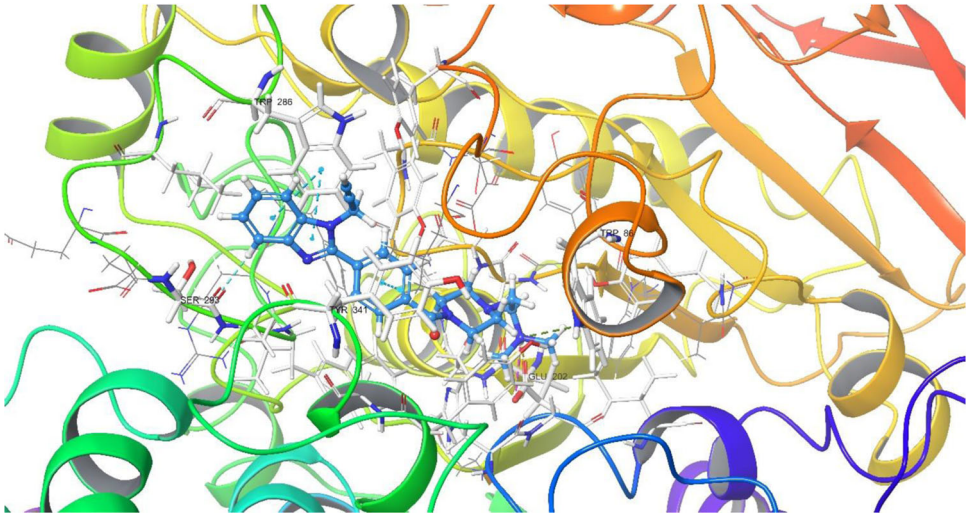

FIGURE 5 Three-dimensional interaction of compound **5g** at the binding region (PBDID: 4EY7). Blue carbons: compound **5g**; white carbons: binding site residues; yellow dashes: H-bond; cyan dashes: aromatic H-bond; blue dashes: π–π interaction; green dashes: π–cation; pink dashes: salt bridge

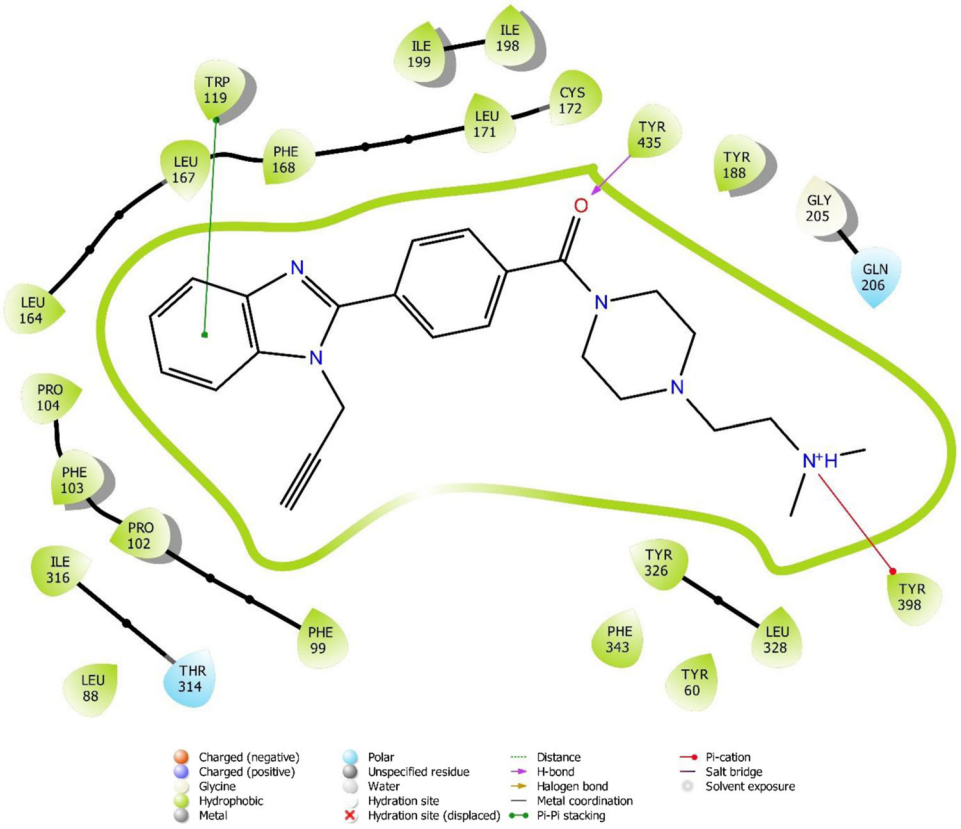

FIGURE 6 Two-dimensional interaction of compound **5g** at the binding region (PBDID: 2V5Z)

square deviations (RMSD) versus time (ns), and the plot of root mean square fluctuation (RMSF) versus residue index were examined. The Rg showed minimal fluctuation (Figure 8a). The lower degree of fluctuation with its consistency during the simulation indicates the greater compactness and rigidity of a system.[45] RMSD is the most commonly used quantitative measure of the similarity between two superimposed atomic coordinates, and in general, changes within 1–3 Å are acceptable for protein structures.[46] In the present study, the RMSD value of the protein was observed to alter by 1.25 Å, which indicates that the protein did not undergo a large

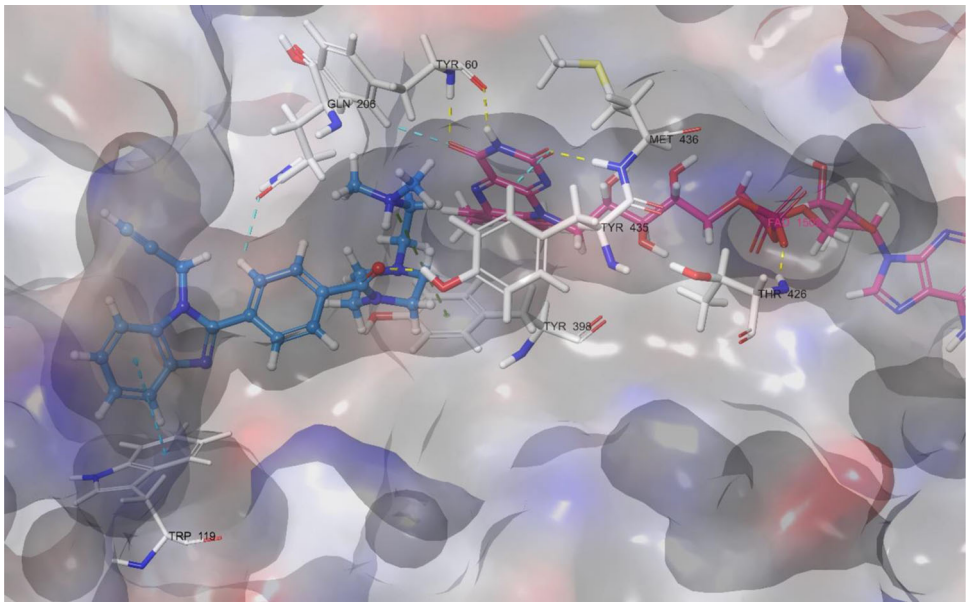

FIGURE 7 Three-dimensional interaction of compound **5g** at the binding region (PBDID: 2V5Z). Blue carbons: compound **5g**; pink carbons: Flavin adenine dinucleotide protein, white carbons: binding site residues; yellow dashes: H-bond; cyan dashes: aromatic H-bond; blue dashes: π–π interaction; green dashes: π–cation. Electrostatic surface (blue-gray-red) was used for the understanding of the shape and the harmony of the protein–ligand complex

conformational change during the simulation (Figure 8b). The low RMSF values confirm that the key binding pocket region is stable.[47] Furthermore, it was expected that α-helices and β-strands should show less fluctuation, but the loop region may show a large fluctuation value.[48] In the present study, the RMSF value of the protein was found to be stable. In fact, the loop region (between 283 and 324 amino acids) was stabilized due to interactions between ligand and enzyme, which demonstrated that ligand and protein powerfully interacted with each other (Figure 8c). In addition, minimum contact strength (cut off 30%) was plotted in 2D to prove how strong the interactions were between ligand and AChE during the entire simulation (Figure 8d). Finally, these results showed that the **5g**–AChE protein complex was stable during the simulation.

In the second step, interaction diagrams of **5g** and AChE (PDB ID:4EY7) were collected (Figure 9, video) and then examined to clarify the relationship between the inhibition activity and the structures. The MDS data showed that **5g** directly interacted with the enzyme through H-bonds, the salt bridge, π–π stacking, and π–π interactions during the simulation (Figure 9a). It was also observed that there were seven aromatic H-bonds between **5g** and Tyr124, Trp286, Arg296, Tyr337, Tyr341, Phe338, and His447 (video). It frequently formed H-bonds with Asp74, Glu202, Phe295, and Arg296 and hydrophobic interactions with Trp86 and Tyr286. These two types of interactions were significantly preserved throughout the simulation (Figure 9b). Additionally, the rest of the hydrophobic interactions were observed between **5g** and Tyr124, Leu289, Phe295, Phe297, Tyr337, Phe338, Tyr341, His447, and Tyr449 amino acids of the protein (Figure 9c).

Docking and MDS studies proved that **5g** fit well in the binding region of the enzyme, which explained why the inhibition effect was high. Moreover, when MDS was applied to the complex obtained from the docking study, it was observed that the ligand–protein complex remained stable. In addition, the H-bond between Phe286 and **5g** and aromatic H-bonds between **5g** and Tyr124, Trp286, Arg296, Tyr337, Tyr341, Phe338, and His447 amino acids were also evinced by the MDS study in contrast to docking. Thus, these findings obtained from the in silico studies supported the in vitro study regarding the inhibition effect of **5g**, which was clarified by the ligand–enzyme relationship.

3 | CONCLUSIONS

AD is one of the most common neurodegenerative diseases. This field is worthy of continued development due to the lack of radical treatment. In recent years, dual inhibitors have attracted interest in the treatment of Alzheimer's disease. To treat it, multifunctional drugs that inhibit both MAO-B and AChE are utilized. Benzimidazole structure with a propargyl side chain, whose selective MAO-B inhibitory activity has already been reported by our laboratory, is still being employed for this purpose. This structure is also planned to interact with the PAS of AChE. The other part of the compounds was substituted with secondary amine derivatives thought to interact favorably with the CAS region of AChE. Piperazine derivatives bearing ACh residues were selected and it was planned to improve the activity. The synthesis of the compounds was carried out in five steps. The benzimidazole ring closure reaction was carried out using microwave conditions. In the synthesis steps, ester–carboxylic acid–acid halide conversions were used. In addition to in vitro

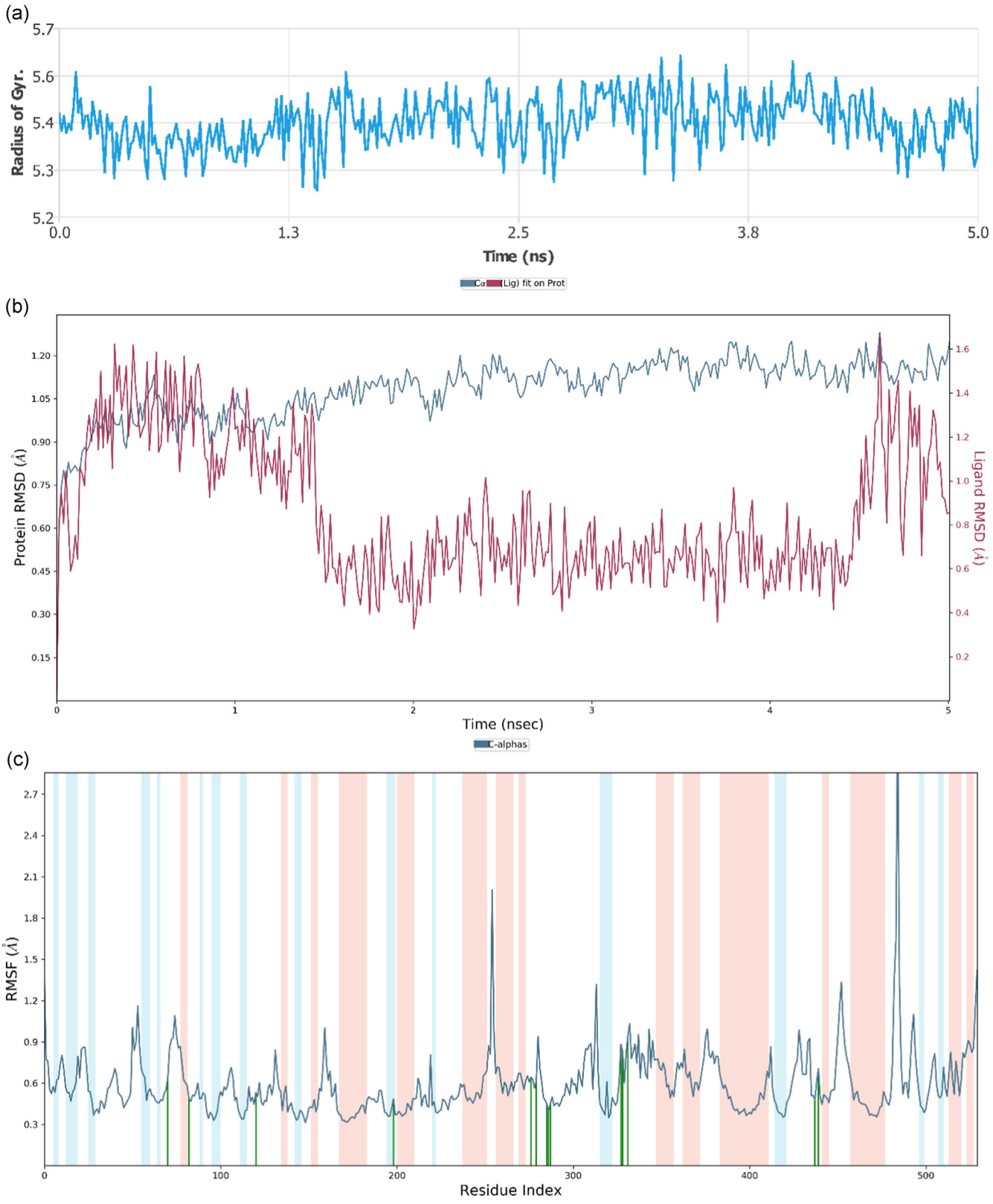

FIGURE 8 Stability diagrams of compound **5g**–acetylcholinesterase complex. (a) Plot of the radius of gyration-time (ns). (b) Plot of root mean square deviation (RMSD) (Å)-time (ns). (c) Plot of root mean square fluctuation (RMSF)-residue index. The areas were represented in light red for the helices, light blue for the strands, and white for the loops. (d) Diagram of the interaction strengths (cut off 30%)

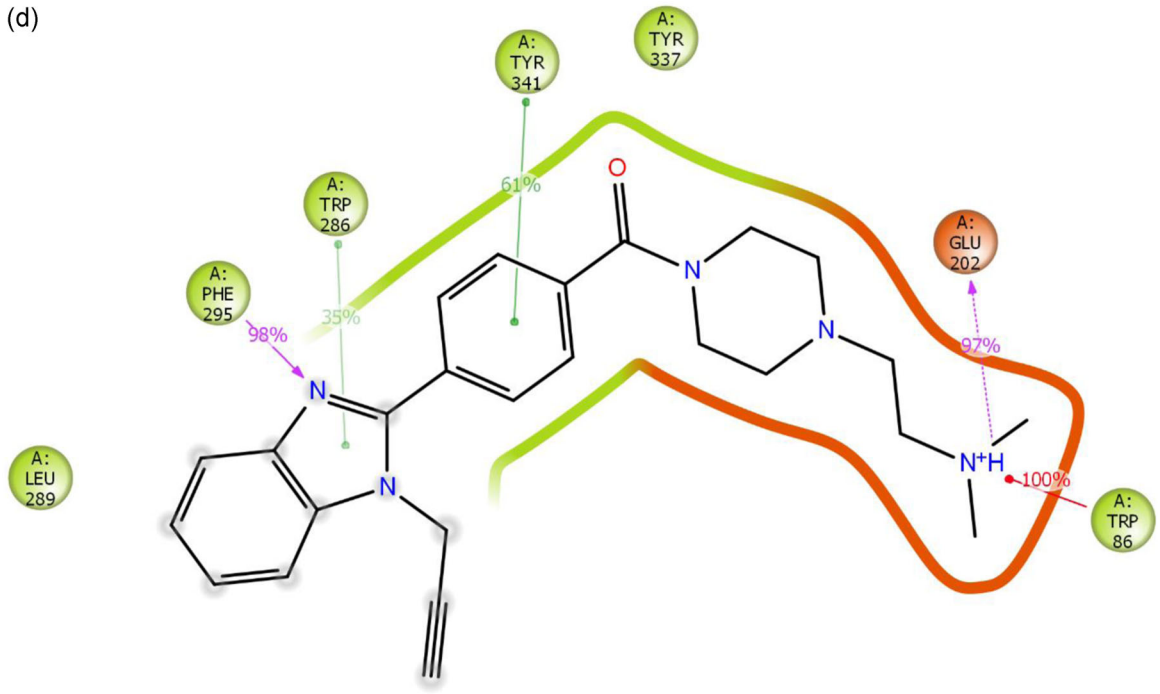

FIGURE 8 Continued

ChE–MAO inhibition tests of the obtained derivatives, inhibition tests of Aβ plaque aggregation, which is an important parameter for Alzheimer's treatment, were performed by means of the in vitro kit procedure. Compound **5g** significantly inhibited Aβ plaque aggregation as well as high AChE–MAO dual inhibition. The docking and dynamic studies carried out clearly determined the interactions of the compounds with the enzyme active site. As planned, the benzimidazole part showed interactions with Trp286 in the PAS region and the piperazine part showed interactions with Trp86 in the CAS region similarly with donepezil. Dynamic studies confirmed that compound **5g** stably binds with the active site of AChE.

4 | EXPERIMENTAL

4.1 | Chemistry

4.1.1 | General

All reagents were purchased from commercial suppliers and were used without further purification. Melting points (M.P.) were determined on the Mettler Toledo-MP90 Melting Point System and were uncorrected. ^{1}H-NMR: Bruker DPX 300 FT-NMR spectrometer; ^{13}C-NMR: Bruker DPX 75 MHz spectrometer (Bruker Bioscience) (please see the Supporting Information). Mass spectra were recorded on a liquid chromatography connected with hybrid ion-trap and time-of-flight mass spectrometry (Shimadzu) using electrospray ionization.

The InChI codes of the investigated compounds, together with some biological activity data, are provided as Supporting Information.

4.1.2 | Synthesis of methyl 4-(1*H*-benzo[*d*]imidazol-2-yl)benzoate (**1**)

Yield: 84%. Benzene-1,2-diamine (0.05 mol) and methyl 4-formyl benzoate (0.05 mol) were stirred in dimethylformamide (DMF) (10 ml) with $Na_2S_2O_5$. The reaction contents were exposed to 10 bar microwave irradiation for 15 min (Monowave 300; Anton-Paar). At the end of the reaction, the mixture was poured into ice water. The precipitated product was filtered, washed with water, dried, and crystallized from ethanol.[39]

4.1.3 | Synthesis of the methyl 4-[1-(prop-2-yn-1-yl)-1*H*-benzo[*d*]imidazol-2-yl]benzoate (**2**)

Yield: 81%. Methyl 4-(1*H*-benzo[*d*]imidazol-2-yl)benzoate (0.039 mol) was dissolved in DMF (20 ml). Sodium hydride (0.046 mol) was added to the reaction mixture in portions. After the addition was complete, the reaction contents were stirred at room temperature until the hydrogen evolution was complete. Afterward, propargyl bromide (0.039 mol) was added to the reaction medium, followed by stirring for 20 h. At the end of the reaction, the mixture was poured into ice water. The precipitated product was filtered, washed with water, dried, and crystallized from ethanol.[39]

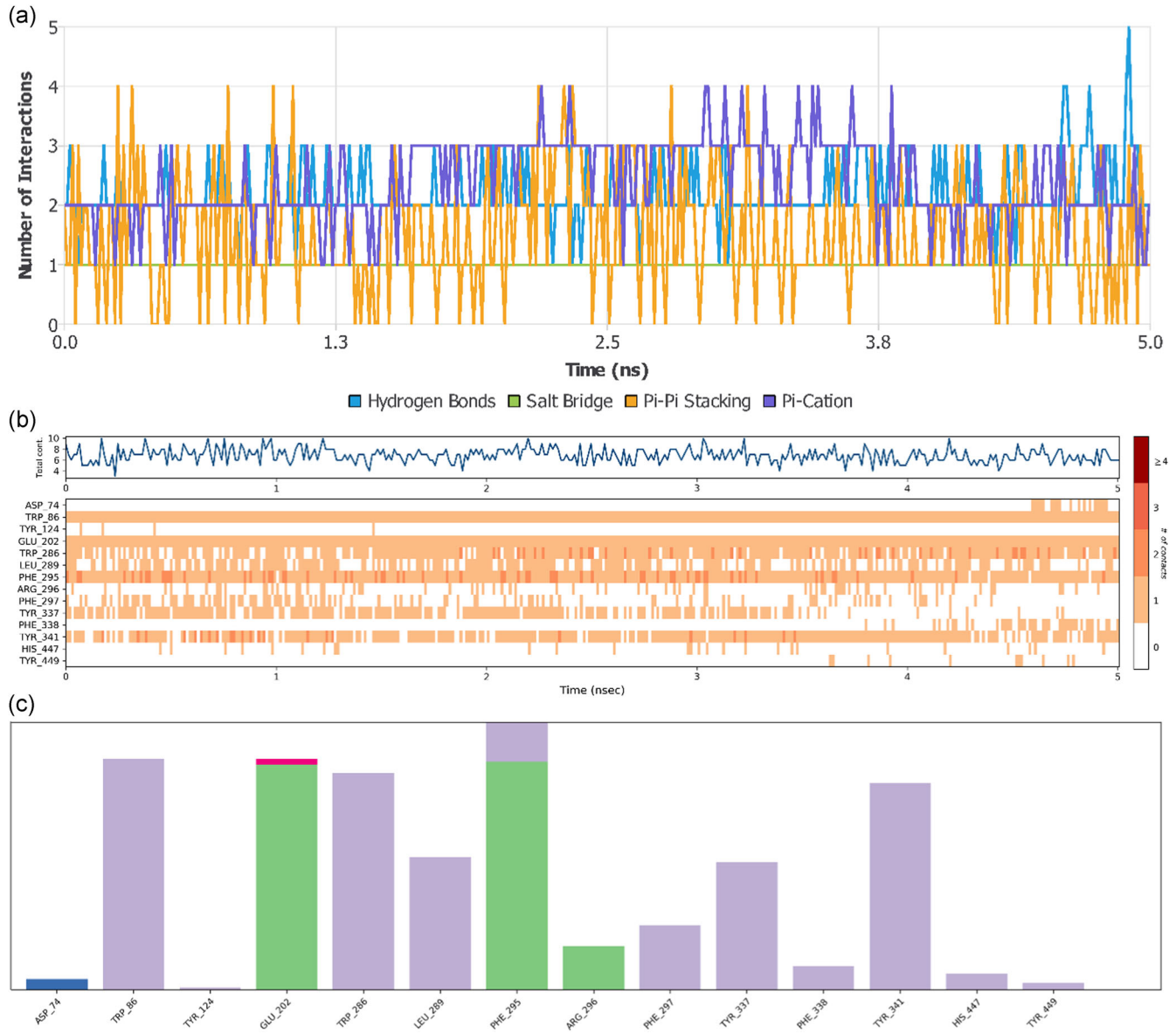

FIGURE 9 Stability checking diagrams of compound **5g**–acetylcholinesterase complex. (a) Number of interactions diagram during the entire simulation. (b) Number of interactions by residue during the simulation. (c) Plot of root mean square fluctuation-residue index (blue: water-mediated H-bond; green: H-bond, pink: ionic interaction, purple: hydrophobic interaction)

4.1.4 | Synthesis of the 4-[1-(prop-2-yn-1-yl)-1*H*-benzo[*d*]imidazol-2-yl]benzoic acid (**3**)

Yield: 90%. Methyl 4-[1-(prop-2-yn-1-yl)-1*H*-benzo[*d*]imidazol-2-yl] benzoate (0.034 mol) was put into a reaction flask. A 3:1 ratio of water/HCl (37%) solution was added, followed by refluxing for 2 h. At the end of the reaction, the mixture was poured into ice water. The precipitated product was filtered, washed with water, and dried.

*4-[1-(Prop-2-yn-1-yl)-1*H*-benzo[*d*]imidazol-2-yl]benzoic acid (**3**)*

Yield: 90%, M.P. = 201.0–202.2°C. ^{1}H-NMR (300 MHz, deuterated dimethyl sulfoxide [DMSO-d_6]): δ = 3.62 (1H, s, –C≡CH), 5.30 (2H, s, –CH_2–), 7.43–7.54 (2H, m, Ar-H), 7.82 (1H, d, J = 7.6 Hz, Ar-H), 7.89 (1H, d, J = 7.6 Hz, Ar-H), 8.04 (2H, d, J = 8.5 Hz, Ar-H), 8.20 (2H, d, J = 8.5 Hz, Ar-H), and 13.45 (1H, br. s, COOH). ^{13}C-NMR (75 MHz, DMSO-d_6): δ = 35.4, 77.6, 78.1, 112.4, 118.2, 124.3, 124.9, 130.0, 130.2, 130.3, 131.3, 133.4, 134.7, 151.0, and 167.1. HRMS (*m/z*): $[M+H]^+$ calcd for $C_{17}H_{12}N_2O_2$: 277.0972; found 277.0975.

4.1.5 | Synthesis of the 4-[1-(prop-2-yn-1-yl)-1*H*-benzo[*d*]imidazol-2-yl]benzoyl chloride (**4**)

After the 4-[1-(prop-2-yn-1-yl)-1*H*-benzo[*d*]imidazol-2-yl]benzoic acid (0.030 mol) was dissolved in 20 ml of thionyl chloride, it was refluxed for 2 h. At the end of the reaction, thionyl chloride was

evaporated under reduced pressure. The remaining product was scraped off and passed to the last step.

*4-[1-(Prop-2-yn-1-yl)-1H-benzo[d]imidazol-2-yl]benzoyl chloride (**4**)*
Yield: 85%, M.P. = 203.3–204.9°C. ^{1}H-NMR (300 MHz, DMSO-d_6): δ = 3.66 (1H, s, –C≡CH), 5.36 (2H, s, –CH_2–), 7.56–7.61 (2H, m, Ar-H), 7.88 (1H, d, J = 7.4 Hz, Ar-H), 8.00 (1H, d, J = 7.7 Hz, Ar-H), 8.04 (2H, d, J = 8.3 Hz, Ar-H), and 8.23 (2H, d, J = 8.3 Hz, Ar-H). ^{13}C-NMR (75 MHz, DMSO-d_6): δ = 35.8, 77.5, 78.2, 113.0, 117.0, 125.8, 125.9, 130.1, 130.4, 130.6, 132.4, 133.8, 134.1, 150.4, and 167.0. HRMS (m/z): $[M+H]^+$ calcd for $C_{17}H_{11}N_2OCl$: 295.0633; found 295.0644.

4.1.6 | Synthesis of the target compounds (**5a–k**)

4-[1-(Prop-2-yn-1-yl)-1*H*-benzo[*d*]imidazol-2-yl]benzoyl chloride (0.001 mol) and secondary amine derivatives (0.001 mol) was reacted in 20 ml acetone with potassium carbonate. At the end of the reaction, acetone was evaporated under reduced pressure. The precipitated product was filtered, washed with water, dried, and crystallized from ethanol.

*(4-Methylpiperazin-1-yl){4-[1-(prop-2-yn-1-yl)-1H-benzo[d]-imidazol-2-yl]phenyl}methanone (**5a**)*
Yield: 82%, M.P. = 232.6–233.2°C. ^{1}H-NMR (300 MHz, DMSO-d_6): δ = 2.21 (3H, s, CH_3), 2.34 (4H, br. s, piperazine CH_2), 3.52 (1H, t, J = 2.3 Hz, –C≡CH), 3.66 (3H, br. s, piperazine CH_2), 5.20 (2H, d, J = 2.3 Hz, CH_2), 7.27–7.39 (2H, m, Ar-H), 7.61 (2H, d, J = 8.3 Hz, Ar-H), 7.68–7.75 (2H, m, Ar-H), and 7.93 (2H, d, J = 8.3 Hz, Ar-H). ^{13}C-NMR (75 MHz, DMSO-d_6): δ = 34.8, 42.0, 46.1, 47.6, 55.0, 76.8, 79.1, 111.4, 119.9, 123.1, 123.5, 127.9, 129.5, 131.0, 135.9, 137.7, 143.3, 152.2, and 168.7. HRMS (m/z): $[M+H]^+$ calcd for $C_{22}H_{22}N_4O$: 359.1866; found 359.1876.

*(4-Ethylpiperazin-1-yl){4-[1-(prop-2-yn-1-yl)-1H-benzo[d]imidazol-2-yl]phenyl}methanone (**5b**)*
Yield: 79%, M.P. = 113.0–113.9°C. ^{1}H-NMR (300 MHz, DMSO-d_6): δ = 1.01 (3H, t, J = 7.2 Hz, CH_3), 2.33–2.42 (6H, m, CH_2, piperazine CH_2), 3.42 (2H, br. s, piperazine CH_2), 3.52 (1H, t, J = 2.4 Hz, –C≡CH), 3.66 (2H, br. s, piperazine CH_2), 5.20 (2H, d, J = 2.4 Hz, CH_2), 7.28–7.39 (2H, m, Ar-H), 7.61 (2H, d, J = 8.4 Hz, Ar-H), 7.70–7.75 (2H, m, Ar-H), and 7.92 (2H, d, J = 8.3 Hz, Ar-H). ^{13}C-NMR (75 MHz, DMSO-d6): δ = 12.3, 34.8, 42.0, 47.6, 51.9, 52.5, 76.8, 79.0, 111.4, 119.9, 123.0, 123.5, 127.9, 129.5, 131.0, 135.9, 137.7, 142.9, 152.1, and 168.7. HRMS (m/z): $[M+H]^+$ calcd for $C_{23}H_{24}N_4O$: 373.2023; found 373.2041.

*[4-(2-Methoxyethyl)piperazin-1-yl]{4-[1-(prop-2-yn-1-yl)-1H-benzo[d]imidazol-2-yl]phenyl}methanone (**5c**)*
Yield: 85%, oily. ^{1}H-NMR (300 MHz, DMSO-d_6): δ = 2.40–2.53 (6H, m, CH_2, piperazine CH_2), 3.22 (3H, s, OCH_3), 3.36 (2H, br. s, piperazine CH_2), 3.52 (1H, s, –C≡CH), 3.64 (2H, br. s, piperazine CH_2), 5.23 (2H, s, CH_2), 7.30–7.37 (2H, m, Ar-H), 7.61 (2H, d, J = 8.3 Hz, Ar-H), 7.70–7.74 (2H, m, Ar-H), and 7.93 (2H, d, J = 8.2 Hz, Ar-H). ^{13}C-NMR (75 MHz, DMSO-d_6): δ = 34.8, 42.5, 47.7, 53.3, 57.3, 58.5, 70.3, 76.8, 79.0, 111.4, 119.9, 123.0, 123.5, 127.9, 129.5, 131.0, 135.9, 137.7, 142.9, 151.2, and 168.7. HRMS (m/z): $[M+H]^+$ calcd for $C_{24}H_{26}N_4O_2$: 397.1459; found 397.1455.

*(4-Isopropylpiperazin-1-yl){4-[1-(prop-2-yn-1-yl)-1H-benzo[d]-imidazol-2-yl]phenyl}methanone (**5d**)*
Yield: 82%, M.P. = 77.0–78.9°C. ^{1}H-NMR (300 MHz, DMSO-d_6): δ = 0.99 (3H, d, J = 6.4 Hz, CH_3), 2.46 (4H, br. s, piperazine CH_2), 2.70 (3H, p, J = 6.4 Hz, CH), 3.39 (2H, br. s, piperazine CH_2), 3.63 (2H, br. s, piperazine CH_2), 3.51 (1H, s, –C≡CH), 5.19 (2H, s, –CH_2–), 7.28–7.38 (2H, m, Ar-H), 7.61 (2H, d, J = 8.0 Hz, Ar-H), 7.70–7.74 (2H, m, Ar-H), and 7.92 (2H, d, J = 8.0 Hz, Ar-H). ^{13}C-NMR (75 MHz, DMSO-d_6): δ = 18.5, 34.8, 42.5, 48.3, 54.2, 77.8, 79.0, 111.4, 119.9, 123.0, 123.5, 127.9, 129.5, 131.0, 135.9, 137.8, 142.9, 152.2, and 168.6. HRMS (m/z): $[M+H]^+$ calcd for $C_{24}H_{26}N_4O$: 387.2179; found 387.2204.

*(4-Allylpiperazin-1-yl){4-[1-(prop-2-yn-1-yl)-1H-benzo[d]imidazol-2-yl]phenyl}methanone (**5e**)*
Yield: 83%, M.P. = 93.6–94.7°C. ^{1}H-NMR (300 MHz, DMSO-d_6): δ = 2.39 (4H, br. s, piperazine CH_2), 2.99 (2H, d, J = 6.4 Hz, CH_2), 3.38 (2H, br. s, piperazine CH_2), 3.53 (1H, t, J = 2.4 Hz, –C≡CH), 3.67 (2H, br. s, piperazine CH_2), 5.13–5.23 (4H, m, CH_2, C═CH_2), 5.78–5.87 (1H, m, HC═C), 7.28–7.39 (2H, m, Ar-H), 7.61 (2H, d, J = 8.3 Hz, Ar-H), 7.70–7.74 (2H, m, Ar-H), and 7.92 (2H, d, J = 8.3 Hz, Ar-H). ^{13}C-NMR (75 MHz, DMSO-d_6): δ = 34.8, 42.0, 47.7, 52.7, 61.1, 76.8, 79.0, 111.4, 118.3, 119.9, 123.0, 123.5, 127.9, 129.5, 130.2, 131.0, 135.6, 135.9, 137.7, 142.9, 152.2, and 168.7. HRMS (m/z): $[M+H]^+$ calcd for $C_{24}H_{24}N_4O$: 385.2023; found 385.2040.

*4-{4-[1-(Prop-2-yn-1-yl)-1H-benzo[d]imidazol-2-yl]benzoyl}-piperazine-1-carbaldehyde (**5f**)*
Yield: 89%, M.P. = 77.8–80.4°C. ^{1}H-NMR (300 MHz, DMSO-d_6): δ = 3.33–3.66 (9H, m, piperazine CH_2, –C≡CH), 5.20 (2H, d, J = 2.3 Hz, CH_2), 7.28–7.9 (2H, m, Ar-H), 7.66 (2H, d, J = 8.4 Hz, Ar-H), 7.70–7.75 (2H, m, Ar-H), 7.94 (2H, d, J = 8.1 Hz, Ar-H), and 8.07 (1H, s, aldehyde CH). ^{13}C-NMR (75 MHz, DMSO-d_6): δ = 34.9, 41.7, 45.2, 76.8, 79.0, 111.4, 119.9, 123.1, 123.5, 128.0, 129.6, 131.2, 135.9, 137.4, 142.9, 152.1, 161.6, and 169.1. HRMS (m/z): $[M+H]^+$ calcd for $C_{22}H_{20}N_4O_2$: 373.1659; found 373.1674.

*{4-[2-(Dimethylamino)ethyl]piperazin-1-yl}{4-[1-(prop-2-yn-1-yl)-1H-benzo[d]imidazol-2-yl]phenyl}methanone (**5g**)*
Yield: 81%, oily. ^{1}H-NMR (300 MHz, DMSO-d_6): δ = 2.17 (6H, s, CH_3), 2.40–2.44 (8H, m, piperazine CH_2, CH_2), 3.43 (2H, br. s, piperazine CH_2), 3.51 (1H, s, –C≡CH), 3.64 (2H, br. s, piperazine CH_2), 5.19 (2H, s, CH_2), 7.28–7.39 (2H, m, Ar-H), 7.61 (2H, d, J = 8.0 Hz, Ar-H), 7.70–7.74 (2H, m, Ar-H), and 7.92 (2H, d, J = 8.0 Hz, Ar-H). ^{13}C-NMR (75 MHz, DMSO-d_6): δ = 34.8, 42.1, 45.9, 47.7, 53.2, 56.0, 56.9, 76.8, 79.0, 111.4, 119.9, 123.1, 123.5, 127.9, 129.5 131.0, 135.9, 137.7, 142.9, 152.1, and 168.6. HRMS (m/z): $[M+H]^+$ calcd for $C_{25}H_{29}N_5O$: 416.2445; found 416.2468.

*{4-[3-(Dimethylamino)propyl]piperazin-1-yl}{4-[1-(prop-2-yn-1-yl)-1H-benzo[d]imidazol-2-yl]phenyl}methanone (**5h**)*

Yield: 80%, M.P. = 71.1–71.9°C. ^{1}H-NMR (300 MHz, DMSO-d_6): δ = 1.56 (2H, p, J = 7.1 Hz, CH_2), 2.11 (6H, s, CH_3), 2.21 (2H, t, J = 7.2 Hz, CH_2), 2.33 (2H, t, J = 7.5 Hz, CH_2), 2.39 (4H, br. s, piperazine CH_2), 3.39 (2H, br. s, piperazine CH_2), 3.53 (1H, t, J = 2.3 Hz, –C≡CH), 3.65 (2H, br. s, piperazine CH_2), 5.19 (2H, d J = 2.3 Hz, CH_2), 7.28–7.39 (2H, m, Ar-H), 7.61 (2H, d, J = 7.3 Hz, Ar-H), 7.70–7.74 (2H, m, Ar-H), and 7.92 (2H, d, J = 7.3 Hz, Ar-H). ^{13}C-NMR (75 MHz, DMSO-d_6): δ = 27.8, 34.8, 45.7, 47.9, 53.3, 56.3, 57.7, 76.8, 79.0, 111.4, 119.9, 123.0, 123.5, 127.9, 129.5, 131.0, 135.9, 137.7, 142.9, 152.2, and 168.6. HRMS (m/z): $[M+H]^+$ calcd for $C_{26}H_{31}N_5O$: 430.2601; found 430.2621.

*(4-Cyclopropylpiperazin-1-yl){4-[1-(prop-2-yn-1-yl)-1H-benzo[d]-imidazol-2-yl]phenyl}methanone (**5i**)*

Yield: 85%, M.P. = 164.7–165.9°C. ^{1}H-NMR (300 MHz, DMSO-d_6): δ = 0.34–0.35 (2H, m, CH_2), 0.43–0.45 (2H, m, CH_2), 1.65–1.71 (1H, m, CH), 2.57 (4H, br. s, piperazine CH_2), 3.38 (2H, br. s, piperazine CH_2), 3.52 (1H, s, –C≡CH), 3.61 (2H, br. s, piperazine CH_2), 5.23 (2H, d, J = 2.0 Hz, CH_2), 7.28–7.38 (2H, m, Ar-H), 7.62 (2H, d, J = 8.2 Hz, Ar-H), 7.70–7.75 (2H, m, Ar-H), and 7.93 (2H, d, J = 8.2 Hz, Ar-H). ^{13}C-NMR (75 MHz, DMSO-d_6): δ = 6.2, 34.9, 38.4, 42.0, 47.6, 53.3, 76.7, 79.0, 111.4, 119.9, 123.0, 123.5, 127.9, 129.5, 131.0, 135.9, 137.7, 142.9, 152.1, and 168.7. HRMS (m/z): $[M+H]^+$ calcd for $C_{24}H_{24}N_4O$: 385.2023; found 385.2050.

*(4-Cyclohexylpiperazin-1-yl){4-[1-(prop-2-yn-1-yl)-1H-benzo[d]-imidazol-2-yl]phenyl}methanone (**5j**)*

Yield: 86%, oily. ^{1}H-NMR (300 MHz, DMSO-d_6): δ = 1.16–1.18 (6H, m, cyclohexyl CH_2), 1.73 (4H, br.s, cyclohexyl CH_2), 2.54 (4H, br.s, piperazine CH_2), 3.50–3.62 (6H, m, piperazine CH_2, cyclohexyl CH, –C≡CH), 5.20 (2H, s, CH_2), 7.28–7.37 (2H, m, Ar-H), 7.60 (2H, d, J = 8.1 Hz, Ar-H), 7.70–7.76 (2H, m, Ar-H), and 7.92 (2H, d, J = 8.1 Hz, Ar-H). ^{13}C-NMR (75 MHz, DMSO-d_6): δ = 25.8, 26.3, 28.7, 34.8, 42.6, 45.4, 48.7, 63.1, 76.8, 79.0, 111.4, 119.9, 123.0, 123.5, 127.9, 129.5, 131.0, 135.9, 137.8, 142.9, 152.1, and 168.5. HRMS (m/z): $[M+H]^+$ calcd for $C_{27}H_{30}N_4O$: 427.2492; found 427.2513.

*(4-Phenylpiperazin-1-yl){4-[1-(prop-2-yn-1-yl)-1H-benzo[d]-imidazol-2-yl]phenyl}methanone (**5k**)*

Yield: 86%, M.P. = 198.6–200.3°C. ^{1}H-NMR (300 MHz, DMSO-d_6): δ = 3.53–3.70 (9H, m, piperazine CH_2, –C≡CH), 5.26 (2H, s, CH_2), 7.05 (2H, d, J = 9.4 Hz, Ar-H), 7.36–7.47 (2H, m, Ar-H), 7.73 (2H, d, J = 8.0 Hz, Ar-H), 7.71–7.82 (2H, m, Ar-H), 7.98 (2H, d, J = 8.1 Hz, Ar-H), and 8.09 (2H, d, J = 9.3 Hz, Ar-H). ^{13}C-NMR (75 MHz, DMSO-d_6): δ = 35.1, 42.6, 44.0, 77.2, 78.7, 111.9, 113.2, 113.9, 119.0, 123.9, 124.2, 126.1, 126.2, 128.2, 129.8, 135.2, 137.6, 138.0, 151.6, 154.9, and 168.9. HRMS (m/z): $[M+H]^+$ calcd for $C_{27}H_{23}N_5O_3$: 466.1874; found 466.1918.

4.2 | Biological assays

4.2.1 | Cholinesterase enzymes inhibition assay

The in vitro AChE and BChE inhibition potencies of the synthesized compounds (**3**, **4**, **5a–k**) were evaluated according to the modified Ellman's spectrophotometric method.[30] The reagents and materials used in the enzyme inhibition assay were supplied commercially by Sigma-Aldrich and Fluka. The cholinesterase enzyme inhibition procedure was applied as reported in our previous research papers.[29,31–37]

4.2.2 | MAO enzymes inhibition assay

The in vitro MAO inhibition test was performed using the available fluorometric method and the percentages and IC_{50} values of the obtained compounds were calculated as previously described by our research group.[38–44]

4.2.3 | Enzyme kinetics studies of the ChE and MAO enzymes

The compound **5g**, which was the most effective derivative in the series against AChE and MAO-B enzymes, was included in the enzyme kinetics study to determine the type of inhibition. For this purpose, this compound was prepared at different concentrations (IC_{50}, 2 × IC_{50}, and IC_{50}/2). The enzyme kinetics assay was carried out as in our previous publications.[29,31–37] Lineweaver–Burk plots were created using Microsoft Office Excel 2013. The K_i values of the compound were easily calculated from the second plot with a common intercept on the x-axis (corresponding to $-K_i$).

4.2.4 | Inhibition of β-amyloid 1–42 (Aβ42) aggregation

The test procedure was created based on the protocol of the β-amyloid 1–42 (Aβ42) ligand screening assay (BioVision), based on the fluorometric method.

4.3 | Molecular docking

Molecular docking studies were performed using an in silico procedure to define the binding modes of active compounds in the active regions of AChE and MAO-B. X-ray crystal structures of the AChE (PDB ID: 4EY7)[49] and MAO-B (PDB ID: 2V5Z)[50] were retrieved from the Protein Data Bank server (www.pdb.org, accessed May 01, 2021). The structures of the enzymes were built using the Schrödinger Maestro[51] interface and were then submitted to the Protein Preparation Wizard protocol of the Schrödinger Suite 2020.

The ligand was prepared using the LigPrep module[52] to correctly assign the protonation states as well as the atom types. Bond orders were assigned, and hydrogen atoms were added to the structures. The grid generation was performed using the Glide module[53] and docking runs were conducted in standard precision docking mode.

4.4 | MDS

MDSs are considered an important computational tool for evaluating the time-dependent stability of a ligand in an active site for a drug–receptor complex.[54] MDSs for 5 ns were carried out to ensure the stability of the identified hits from the docking result. We performed the Desmond application[48] using the standard force field (OPLS3e) of the Schrodinger Suite with a transferable intermolecular potential with a 3-points (TIP3P) water model followed by energy minimization of the complex.[55] The neutralization of the system was achieved using Na^+ and Cl^- ions. MDS was performed following the completion of the system setup. Rg, RMSF, and RMSD values were calculated by the Desmond application.[48]

ACKNOWLEDGMENT

As the authors of this study, we thank the Anadolu University Faculty of Pharmacy Doping and Narcotic Substances Laboratory for their support and contributions.

CONFLICT OF INTERESTS

The authors declare that there are no conflicts of interests.

ORCID

Derya Osmaniye http://orcid.org/0000-0002-0499-436X
Serkan Levent http://orcid.org/0000-0003-3692-163X
Yusuf Özkay http://orcid.org/0000-0001-8815-153X
Zafer A. Kaplancıklı https://orcid.org/0000-0003-2252-0923

REFERENCES

[1] L. Cahlíková, R. Vrabec, F. Pidaný, R. Peřinová, N. Maafi, A. A. Mamun, A. Ritomská, V. Wijaya, G. Blunden, *Molecules* **2021**, *26*, 5240.
[2] T. Mazej, D. Knez, A. Meden, S. Gobec, M. Sova, *Molecules* **2021**, *26*, 4118.
[3] J. Guo, Y. Zhang, C. Zhang, C. Yao, J. Zhang, X. Jiang, Z. Zhong, J. Ge, T. Zhou, R. Bai, *Bioorg. Chem.* **2021**, *113*, 105013.
[4] T. Behl, D. Kaur, A. Sehgal, S. Singh, N. Sharma, G. Zengin, F. L. Andronie-Cioara, M. M. Toma, S. Bungau, A. G. Bumbu, *Molecules* **2021**, *26*, 3724.
[5] C. Hu, L. Jiang, L. Tang, M. Zhang, R. Sheng, *Bioorg. Med. Chem.* **2021**, *44*, 116306.
[6] K. Wang, J. Shi, Y. Zhou, Y. He, J. Mi, J. Yang, S. Liu, X. Tang, W. Liu, Z. Tan, *Bioorg. Chem.* **2021**, *112*, 104879.
[7] T. H. Ferreira-Vieira, I. M. Guimaraes, F. R. Silva, F. M. Ribeiro, *Curr. Neuropharmacol.* **2016**, *14*, 101.
[8] Z. Zhang, J. Guo, M. Cheng, W. Zhou, Y. Wan, R. Wang, Y. Fang, Y. Jin, J. Liu, S. S. Xie, *Eur. J. Med. Chem.* **2021**, *213*, 113154.
[9] Z. Sang, Q. Song, Z. Cao, Y. Deng, Z. Tan, L. Zhang, *Eur. J. Med. Chem.* **2021**, *216*, 113310.
[10] Z. Cao, Q. Song, G. Yu, Z. Liu, S. Cong, Z. Tan, Y. Deng, *Bioorg. Med. Chem.* **2021**, *35*, 116074.
[11] S. Carradori, R. Silvestri, *J. Med. Chem.* **2015**, *58*, 6717.
[12] C. A. Cobb, M. P. Cole, *Neurobiol. Dis.* **2015**, *84*, 4.
[13] J. Guo, Z. Mi, X. Jiang, C. Zhang, Z. Guo, L. Li, J. Gu, T. Zhou, R. Bai, Y. Xie, *Bioorg. Chem.* **2021**, *108*, 104564.
[14] A. H. Hasan, S. I. Amran, F. H. Saeed Hussain, B. A. Jaff, J. Jamalis, *ChemistrySelect* **2019**, *4*, 14140.
[15] S. Bal, Ö. Demirci, B. Şen, P. Taslimi, A. Aktaş, Y. Gök, M. Aygün, İ. Gülçin, *Arch. Pharm.* **2021**, *354*, 2000422.
[16] A. Latif, S. Bibi, S. Ali, A. Ammara, M. Ahmad, A. Khan, A. Al-Harrasi, F. Ullah, M. Ali, *Drug Dev. Res.* **2021**, *82*, 207.
[17] S. C. Raka, A. Rahman, F. Hussain, S. A. Rahman, *Saudi J. Biol. Sci.* **2021**, *28*, 12.
[18] L. Dinparast, G. Zengin, M. B. Bahadori, *Biointerface Res. Appl. Chem.* **2021**, *11*, 10739.
[19] B. Adalat, F. Rahim, M. Taha, F. J. Alshamrani, E. H. Anouar, N. Uddin, S. A. A. Shah, Z. Ali, Z. A. Zakaria, *Molecules* **2020**, *25*, 4828.
[20] A. S. Gurjar, V. S. Solanki, A. R. Meshram, S. S. Vishwakarma, *J. Chin. Chem. Soc.* **2020**, *67*, 864.
[21] J. Mo, T. Chen, H. Yang, Y. Guo, Q. Li, Y. Qiao, H. Lin, F. Feng, W. Liu, Y. Chen, *J. Enzyme Inhib. Med. Chem.* **2020**, *35*, 330.
[22] S. Ali, M. H. H. B. Asad, S. Maity, W. Zada, A. A. Rizvanov, J. Iqbal, B. Babak, I. Hussain, *Bioorg. Chem.* **2019**, *88*, 102936.
[23] Y. Fang, H. Zhou, Q. Gu, J. Xu, *Eur. J. Med. Chem.* **2019**, *167*, 133.
[24] M. Krátký, Q. A. Vu, Š. Štěpánková, A. Maruca, T. B. Silva, M. Ambrož, V. Pflégr, R. Rocca, K. Svrčková, S. Alcaro, *Bioorg. Chem.* **2021**, *116*, 105301.
[25] M. do Carmo Carreiras, L. Ismaili, J. Marco-Contelles, *Bioorg. Med. Chem. Lett.* **2020**, *30*, 126880.
[26] Y.x Xu, H. Wang, X.k Li, S.n Dong, W. Liu, Q. Gong, Y. Tang, J. Zhu, J. Li, H.y Zhang, *Eur. J. Med. Chem.* **2018**, *143*, 33.
[27] U. Košak, D. Knez, N. Coquelle, B. Brus, A. Pišlar, F. Nachon, X. Brazzolotto, J. Kos, J.-P. Colletier, S. Gobec, *N*, *Bioorg. Med. Chem.* **2017**, *25*, 633.
[28] Ö. D. Can, D. Osmaniye, Ü. D. Özkay, B. N. Sağlık, S. Levent, S. Ilgın, Y. Ozkay, Z. A. Kaplancıklı, *Eur. J. Med. Chem.* **2017**, *131*, 92.
[29] B. N. Sağlık, S. Ilgın, Y. Özkay, *Eur. J. Med. Chem.* **2016**, *124*, 1026.
[30] G. L. Ellman, K. D. Courtney, V. Andres, R. M. Featherstone Jr., *Biochem. Pharmacol.* **1961**, *7*, 88.
[31] Ü. D. Özkay, Ö. D. Can, B. N. Sağlık, U. A. Çevik, S. Levent, Y. Özkay, S. Ilgın, Ö. Atlı, *Bioorg. Med. Chem. Lett.* **2016**, *26*, 5387.
[32] U. Acar Cevik, S. Levent, B. Nurpelin Saglık, Y. Ozkay, Z. Asım Kaplancıklı, *Lett. Drug Des. Discov.* **2017**, *14*, 528.
[33] S. Levent, U. Acar Çevik, B. N. Sağlık, Y. Özkay, Ö. D. Can, Ü. D. Özkay, Ü. Uçucu, *Phosphorus Sulfur Silicon Relat. Elem.* **2017**, *192*, 469.
[34] W. Hussein, B. N. Sağlık, S. Levent, B. Korkut, S. Ilgın, Y. Özkay, Z. A. Kaplancıklı, *Molecules* **2018**, *23*, 2033.
[35] U. Acar Cevik, B. N. Saglik, S. Levent, D. Osmaniye, B. Kaya Cavuşoglu, Y. Ozkay, Z. A. Kaplancikli, *Molecules* **2019**, *24*, 861.
[36] D. Osmaniye, B. N. Sağlık, U. Acar Çevik, S. Levent, B. Kaya Çavuşoğlu, Y. Özkay, Z. A. Kaplancıklı, G. Turan, *Molecules* **2019**, *24*, 2392.
[37] F. Tok, B. Koçyiğit-Kaymakçıoğlu, B. N. Sağlık, S. Levent, Y. Özkay, Z. A. Kaplancıklı, *Bioorg. Chem.* **2019**, *84*, 41.
[38] B. N. Sağlık, B. K. Çavuşoğlu, D. Osmaniye, S. Levent, U. A. Çevik, S. Ilgın, Y. Özkay, Z. A. Kaplancıklı, Y. Öztürk, *Bioorg. Chem.* **2019**, *85*, 97.
[39] Ö. D. Can, D. Osmaniye, Ü. D. Özkay, B. N. Sağlık, S. Levent, S. Ilgın, M. Baysal, Y. Özkay, Z. A. Kaplancıklı, *Eur. J. Med. Chem.* **2017**, *131*, 92.

[40] N. Ö. Can, D. Osmaniye, S. Levent, B. N. Sağlık, B. Korkut, Ö. Atlı, Y. Özkay, Z. A. Kaplancıklı, *Eur. J. Med. Chem.* **2018**, *144*, 68.
[41] S. Ilgın, D. Osmaniye, S. Levent, B. N. Sağlık, U. Acar Çevik, B. K. Çavuşoğlu, Y. Özkay, Z. A. Kaplancıklı, *Molecules* **2017**, *22*, 2187.
[42] N. Ö. Can, D. Osmaniye, S. Levent, B. N. Sağlık, B. Inci, S. Ilgın, Y. Özkay, Z. A. Kaplancıklı, *Molecules* **2017**, *22*, 1381.
[43] F. Tok, Z. Uğraş, B. N. Sağlık, Y. Özkay, Z. A. Kaplancıklı, B. Koçyiğit-Kaymakçıoğlu, *Bioorg. Chem.* **2021**, *112*, 104917.
[44] F. Tok, B. N. Sağlık, Y. Özkay, S. Ilgın, Z. A. Kaplancıklı, B. Koçyiğit-Kaymakçıoğlu, *Bioorg. Chem.* **2021**, *114*, 105038.
[45] R. Islam, M. R. Parves, A. S. Paul, N. Uddin, M. S. Rahman, A. A. Mamun, M. N. Hossain, M. A. Ali, M. A. Halim, *J. Biomol. Struct. Dyn.* **2021**, *39*, 3213.
[46] N. P. Sangai, C. N. Patel, H. A. Pandya, *Toxicol. Res.* **2018**, *7*, 1091.
[47] I. Aier, P. K. Varadwaj, U. Raj, *Sci. Rep.* **2016**, *6*(34984), 1.
[48] Schrödinger, LLC, *Schrödinger suite*, Schrödinger, LLC, New York, NY **2020**.
[49] J. Cheung, M. J. Rudolph, F. Burshteyn, M. S. Cassidy, E. N. Gary, J. Love, M. C. Franklin, J. J. Height, *J. Med. Chem.* **2012**, *55*, 10282.
[50] S. Y. Son, J. Ma, Y. Kondou, M. Yoshimura, E. Yamashita, T. Tsukihara, *Proc. Natl. Acad. Sci.* **2008**, *105*, 5739.
[51] Schrödinger, LLC, *Maestro*, *10.6*, Schrödinger, LLC, New York, NY **2020**.
[52] Schrödinger, LLC, *LigPrep*, *version 3.8*, Schrödinger, LLC, New York, NY **2020**.
[53] Schrödinger, LLC, *Glide*, *version 7.1*, Schrödinger, LLC, New York, NY **2020**.
[54] X. Liu, D. Shi, S. Zhou, H. Liu, H. Liu, X. Yao, *Expert Opin. Drug Discov.* **2018**, *13*, 23.
[55] B. Sureshkumar, Y. S. Mary, K. Resmi, S. Suma, S. Armaković, S. J. Armaković, C. van Alsenoy, B. Narayana, D. Sobhana, *J. Mol. Struct.* **2018**, *1167*, 95.

SUPPORTING INFORMATION

Additional supporting information may be found in the online version of the article at the publisher's website.

How to cite this article: D. Osmaniye, A. E. Evren, B. N. Sağlık, S. Levent, Y. Özkay, Z. A. Kaplancıklı, *Arch. Pharm.* **2022**;355:e2100450.
https://doi.org/10.1002/ardp.202100450